Full Paper
doi.org/10.1002/ejoc.202001165

Expanded Porphyrinoids | *Very Important Paper* |

Synthesis and Structure of *meso*-Substituted Dibenzihomoporphyrins

Nitika Grover,[a] Ganapathi Emandi,[a] Brendan Twamley,[b] Bhavya Khurana,[c,d] Vincent Sol,[d] and Mathias O. Senge*[c,e]

Dedicated to Professor Tavarekere K. Chandrashekar on the occasion of his 65th birthday

Abstract: Bench-stable meso-substituted di(*p*/*m*-benzi)homoporphyrins were synthesized through acid-catalyzed condensation of dipyrrole derivatives with aryl aldehydes. The insertion of a 1,1,2,2-tetraphenylethene (TPE) or but-2-ene-2,3-diyldibenzene unit in the porphyrin framework results in the formation of dibenzihomoporphyrins, merging the features of hydrocarbons and porphyrins. Single crystal X-ray analyses established the non-planar structure of these molecules, with the phenylene rings out of the mean plane, as defined by the dipyrromethene moiety and the two meso-carbon atoms. Spectroscopic and structural investigations show that the macrocycles exhibit characteristics of both TPE or but-2-ene-2,3-diyldibenzene and dipyrromethene units indicating the non-aromatic characteristics of the compounds synthesized. Additionally, the dibenzihomoporphyrins were found to generate singlet oxygen, potentially allowing their use as photosensitizers.

Introduction

The synthetic chemistry of expanded porphyrinoids has attracted considerable attention for the last twenty-five years.[1] Studies on macrocycles related to porphyrins have been prompted by their fascinating structure, flexible conformation, aromaticity, and unique coordination chemistry.[2] Expanded porphyrinoids have more than 18π-electrons in their conjugation pathway, which uniquely alters the reactivity of the macrocyclic core. Due to their special electronic and structural properties, expanded porphyrinoids are used in various applications such as non-linear optics (NLO),[3a] photodynamic therapy (PDT),[3b] and ion recognition.[3c]

The simplest expanded, conjugated analog of [18]-porphyrin(1.1.1.1) **1** is [20]-porphyrin(2.1.1.1) or [20π]-homoporphyrin **2** that exhibits five meso carbons and four pyrrole rings (Figure 1). In contrast to normal porphyrins, [20π]-homoporphyrins are non-aromatic. In 1971, Grigg reported the first azahomoporphyrin **3**; however, this compound was found to be unstable and rearranged to the respective aziridine-fused porphyrin with only one sp^3-carbon in the macrocycle.[4] Subsequent synthetic efforts by Callot and co-workers and structural studies from Weiss's group established the first [20π]-homoporphyrin **4**.[5] The latter compound was also unstable and decomposed even in the solid-state.

Eventually, the synthesis of bench-stable core-modified [20π]-homoporphyrins (such as **5**) was reported by Ravikanth and co-workers.[6] 40 years after their initial discovery, the synthesis and coordination properties of fully conjugated [20π]-homoporphyrin derivatives **6** with Möbius topology was reported by Srinivasan and co-workers.[7]

Another class of porphyrin analogs, in which one or more pyrrole rings is replaced by a benzene ring, is known as benziporphyrin.[8] Diverse benziporphyrin structures ranging from non-aromatic to highly diatropic species have been reported and they are used as surrogate ligands in place of porphyrins, especially for heavy transition metals. Additionally, benzipor-

[a] *Dr. N. Grover, Dr. G. Emandi*
School of Chemistry, Trinity College Dublin, The University of Dublin, Trinity Biomedical Sciences Institute, 152-160 Pearse Street, Dublin 2, Ireland
[b] *Dr. B. Twamley*
School of Chemistry, Trinity College Dublin, The University of Dublin, Dublin 2, Ireland
[c] *B. Khurana, Prof. Dr. M. O. Senge*
Medicinal Chemistry, Trinity Translational Medicine Institute, Trinity Centre for Health Sciences, Trinity College Dublin, The University of Dublin, St James's Hospital, Dublin 8, Ireland
[d] *B. Khurana, Prof. Dr. V. Sol*
Université de Limoges, Laboratoire PEIRENE, EA 7500 87000 Limoges, France
[e] *Prof. Dr. M. O. Senge*
Institute for Advanced Study (TUM-IAS) Technical University of Munich Lichtenbergstrasse 2a, 85748 Garching, Germany
E-mail: mathias.senge@tum.ie
https://chemistry.tcd.ie/staff/people/mos/Home.html

Supporting information and ORCID(s) from the author(s) for this article are available on the WWW under https://doi.org/10.1002/ejoc.202001165.

Full Paper
doi.org/10.1002/ejoc.202001165

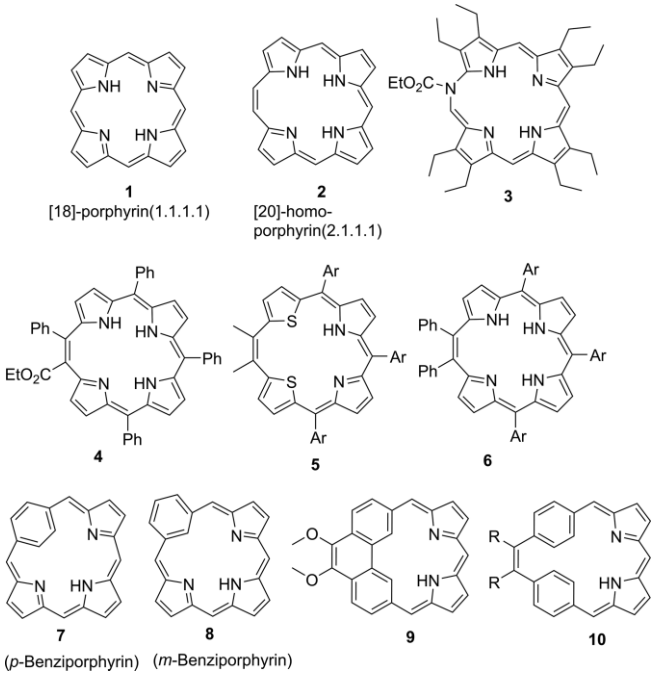

Figure 1. Fundamental structures of porphyrins, homoporphyrins, benziporphyrins and target systems.

phyrins are hypothesized to stabilize metals in unusual oxidation states. Benziporphyrins are classified into two sub-types: (a) *p*-benziporphyrin **7** where the benzene ring is attached via a 1,4-phenylene linkage and (b) *m*-benziporphyrin **8** with attachment via a 1,3-phenylene linkage. The aromaticity of benziporphyrins is highly dependent upon the way this phenylene is linked into the macrocycle.[9,10] In general, *m*-benziporphyrins are non-aromatic, whereas *p*-benziporphyrins preserve the aromatic characters of porphyrin. The electronic properties of benziporphyrins can be manipulated through core modification, meso-substitution, and metal coordination.

Considering these precedents of porphyrin-inspired macrocycles, we envisioned the synthesis of a new class of porphyrin that exhibits combined structural features of homoporphyrins and benziporphyrins, i.e. di(*p*/*m*-benzi)homoporphyrins. Although structurally characterized dibenzicorroles are known in the literature, they are strictly limited to incorporation of polycyclic aromatic hydrocarbons in the macrocycle, as shown for system **9** (Figure 1).[11] meso-Substituted benzihomoporphyrins of type **10** have not been reported in the literature. Additionally, porphyrins and related compounds are often singlet oxygen-generating photosensitizers of note. However, π-conjugated expanded porphyrins tend to aggregation which significantly decreases the singlet oxygen quantum yield.[12] While this can be counteracted by steric shielding, e.g., in nanostructures and out-of-plane coordinated porphyrins,[12,13] conformational distortion may also negatively impact this.[14]

Herein we report the synthesis of meso-substituted dibenzihomoporphyrins, which contain phenyl or methyl substituents at the vinylene bridge and aryl substituents at the meso positions to control the conformational and electronic properties of the macrocycles. To compare the structural and electronic features, we targeted the synthesis of di(*p*-benzi)homoporphyrins and di(*m*-benzi)homoporphyrins which was achieved by introducing *p*- or *m*-phenylene unit in the porphyrin framework.

Results and Discussion

Synthesis

The synthesis of meso-substituted di(*p*-benzi)homoporphyrins is outlined in Scheme 1. In the first step, a McMurry coupling reaction was employed for the conversion of 4-bromobenzophenone (**11**) to 1,2-bis(4-bromophenyl)-1,2-diphenylethene **13**.[15] In the next step, (1,2-diphenylethene-1,2-diyl)bis-(4,1-phenylene))bis((4-methoxyphenyl)methanol) **15** was synthesized through reaction of 1,2-bis(4-bromophenyl)-1,2-diphenylethene **13** with *n*BuLi followed by addition of *p*-anisaldehyde. The synthesis of key dipyrrolic intermediate **17** was achieved by reaction of excess pyrrole with **15** in the presence of a catalytic amount of $BF_3{\cdot}Et_2O$. In the final step, the acid-catalyzed condensation of **17** with pentafluorobenzaldehyde followed by oxidation with DDQ afforded the desired compound **19**.

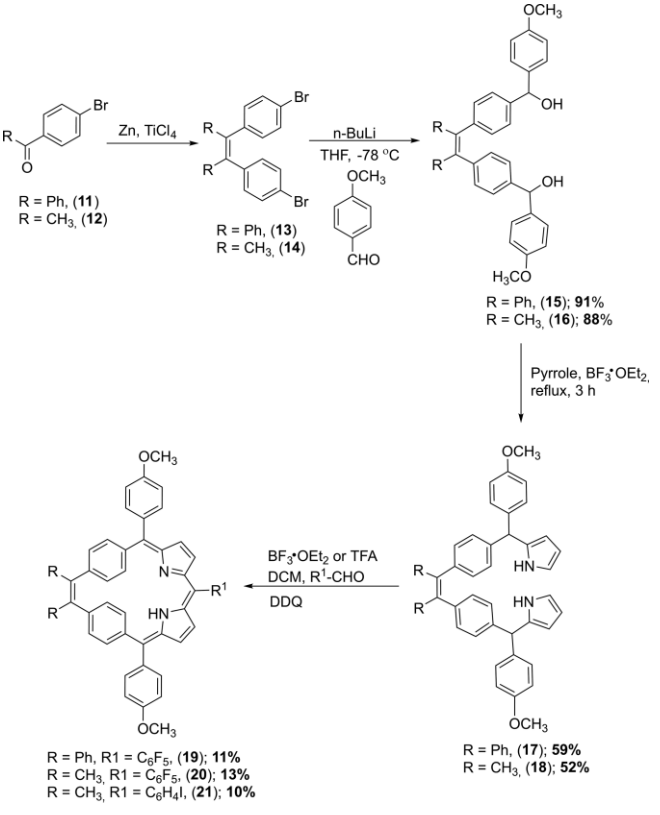

Scheme 1. Synthesis of *meso*-substituted di(*p*-benzi)homoporphyrins.

Different reaction conditions were trialed to obtain the maximum possible yield of compound **19**. We observed the reaction of dipyrrole **17** with pentafluorobenzaldehyde in the presence of 1.0 equiv. of $BF_3{\cdot}Et_2O$ at room temperature for 15 h, providing the final compound **19** in 11 % yield. Similarly, a reaction of compound **17** with pentafluorobenzaldehyde and 1.0 equiv.

Full Paper
doi.org/10.1002/ejoc.202001165

of TFA yielded compound **19** in 12 % yield. However, the use of 2.5 equiv. acids (BF_3•Et_2O or TFA) significantly decreased the yield to 5–8 %. To further study the versatility of reaction conditions, we synthesized compounds **20** and **21**. The synthesis of compound **20** started with the McMurry reaction of 1-(4-bromophenyl)ethanone (**12**) to yield 4,4′-(but-2-ene-2,3-diyl)bis(bromobenzene) **14**. Diol **16** and dipyrrole **18** were synthesized using the reaction conditions described earlier.[7b]

A condensation reaction of dipyrrole **18** with pentafluorobenzaldehyde yielded **20** in 13 % isolated yield. In a similar vein, compound **21** was afforded in 10 % yield using a reaction of dipyrrole **18** with 4-iodobenzaldehyde. The yields obtained in this project are in good agreement with reports documented in the literature.[6a,7b]

Building upon the progress made in synthetically accessing di(*p*-benzi)homoporphyrins, we extended our efforts towards the synthesis of the related di(*m*-benzi)homoporphyrins. The synthesis of the target compounds **26**, **27**, and **28** is outlined in Scheme 2. In a similar manner to that outlined above, we started with the transformation of 1-(3-bromophenyl)ethanone **22** to 3,3′-(but-2-ene-2,3-diyl)bis(bromobenzene) **23** using standard McMurry conditions.[16] Furthermore, a reaction of **23** with *n*BuLi and 4-anisaldehyde proceeded smoothly to access diol **24** in 83 % yield. A reaction of the diol **24** with 40 equiv. of pyrrole in the presence of BF_3•Et_2O gave the dipyrrole **25** in 46 % yield. A preliminary screen of the substrate scope was investigated by incorporating combinations of structural motifs such as pentafluorophenyl anthracenyl or 4-iodophenyl groups to access the macrocycles **26**, **27**, and **28**.

The synthesized compounds were characterized using 1D/2D NMRs, MALDI-TOF-MS, UV/Vis spectroscopy, and single-crystal X-ray analysis. The NMR spectra in $CDCl_3$ and mass spectra of **19**, **20**, **21**, **26**, **27**, and **28** are shown in Figures S1–S21 in the supporting information (SI). Figure 2 gives the ^{1}H NMR

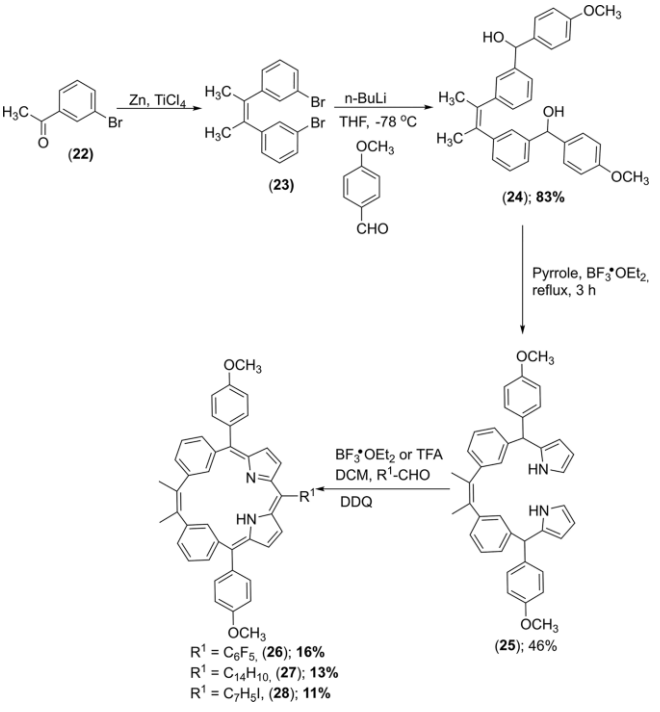

Scheme 2. Synthesis of *meso*-substituted di(*m*-benzi)homoporphyrins.

spectrum of compound **19** and is consistent with the structure of **19** as being built of a TPE moiety linked with a meso-pentafluorophenyldipyrromethene unit through two 4-methoxyphenylmethine bridges. The ^{1}H NMR spectrum of **19** shows a significant downfield shift of the inner core NH at δ = 12.55 ppm. The β-pyrrolic protons appear with two sets of doublets (J = 5.2 Hz) at δ = 6.47 and 5.80 ppm. These preliminary details indicate that the effective π-conjugation is interrupted in the dibenzihomoporphyrin **19**.

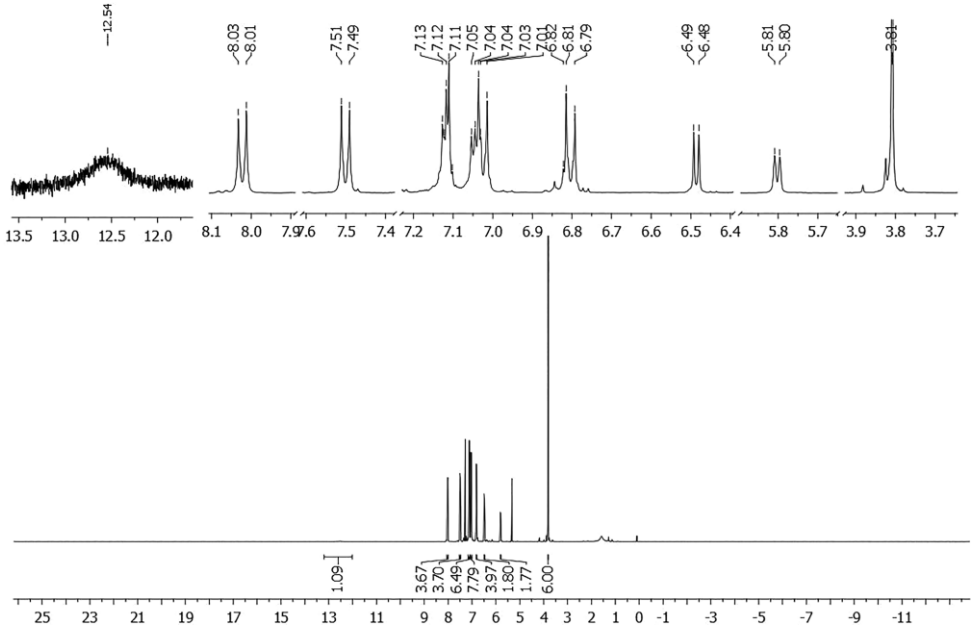

Figure 2. ^{1}H NMR spectrum of compound **19** in $CDCl_3$.

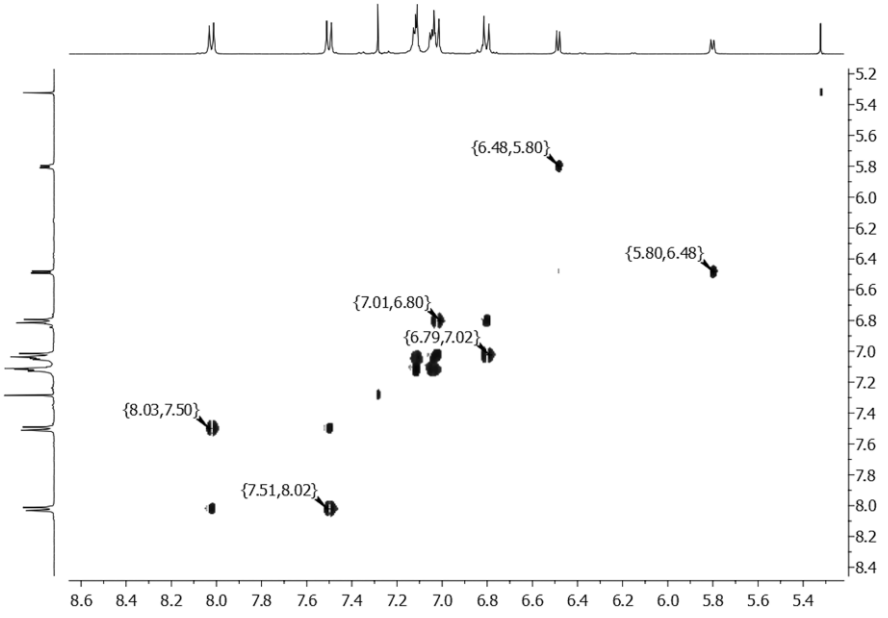

Figure 3. ^{1}H-^{1}H COSY spectrum of compound **19** in $CDCl_3$.

These results are also supported by the 2D NMR spectra. The ^{1}H-^{1}H COSY NMR spectrum of compound **19** in Figure 3 shows the correlation between the peaks; (i) 8.03 and 7.50 ppm (ii) 7.01 and 6.80 ppm (iii) 6.48 and 5.80. Overall, the spectral results for **19** are in closed agreement with the reported non-aromatic porphyrin surrogates. Similar results were observed for the other synthesized porphyrin frameworks (**20**, **21**, **26**, **27**, and **28**)**.**

Absorption spectra of **19**, **20**, **21**, **26**, **27**, and **28** were recorded in CH_2Cl_2 at 298 K. These compounds show two distinct absorptions; a strong sharp band (350–400 nm) and a weak broad band (550–800 nm), reflecting the non-aromatic nature of macrocyclic ring.[17a] The latter band in compound **20** is ca. 10 nm red-shifted compared to compound **19,** whereas the same band in **21** is ca. 7 nm red-shifted compared to **19**. The long-wavelength absorbing band in the absorption spectra of di(*m*-benzi)homoporphyrins is blue-shifted compared to the corresponding di(*p*-benzi)homoporphyrins. These shifts and trends in absorption spectra reflect the combined effects of meso-substitution, 1,4-phenylene, and, 1,3-phenylene linkages**.** Figure 4 gives an example of the absorption spectrum of compound **19** and the respective protonated species. The addition of TFA to a solution of homobenziporphyrins resulted in a red-shift in their absorption spectra; for example, the long-wavelength absorbing band for **19** + TFA is ca. 150 nm red-shifted compared to **19**. Similar trends were observed for compounds **20**, **21**, **26**, **27**, and **28;** corresponding spectra are given in Figures S22–S23 in the SI.

The redshift upon protonation depends on the extent of the out-of-plane deformation of the macrocyclic core. Out-of-plane deformation leads to destabilization of the HOMOs followed by a reduction of the HOMO-LUMO gap hence, a redshift in absorption spectra observed.[17b] Additionally, it was observed that porphyrins with electron-donating groups at meso-positions also exhibit large bathochromic shifts.[17c] Therefore, the

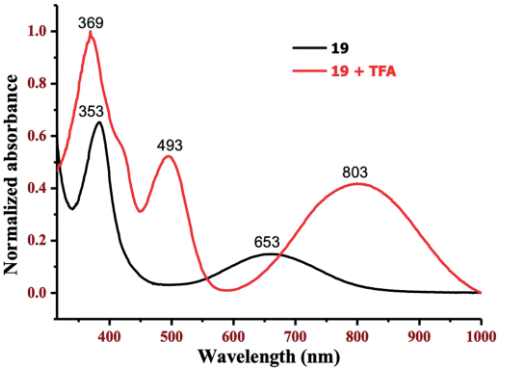

Figure 4. Comparative absorption spectra of **19** and protonated species (**19**+TFA) in $CHCl_3$.

large red-shift upon protonation observed for dibenzihomoporphyrin derivatives is a combined result of protonation induced steric deformation of the macrocycle and electronic effect of the 4-methoxyphenyl groups.

Crystallography

The structures of **19**, **20**, and **27** were confirmed by single-crystal X-ray analysis. Compound **19** crystallized in the monoclinic lattice system with a $P\bar{1}$ space group (Figure 5). The dipyrromethene unit of the di(*p*-benzi)homoporphyrin **19** is planar and exhibits bond lengths between 1.30 Å to 1.45 Å which indicate the delocalization of the π-electrons. In contrast to the dipyrromethene unit, the *p*-phenylene units are out of the plane defined by the dipyrromethene moiety and the two meso-carbons, effectively interrupting π-conjugation in the macrocycle. The bond lengths in the 1,2-bisphenyl-1,2-bis-*p*-phenyleneethene unit are in the range of 1.47–1.48 Å, indicating more double bond than aromatic bond character. The angle

Full Paper
doi.org/10.1002/ejoc.202001165

between *p*-phenylene ring A and the dipyrromethene unit is 51.2(1)° whereas the angle between *p*-phenylene ring B and the dipyrromethene unit is 54.7(1)° (Figure 5).

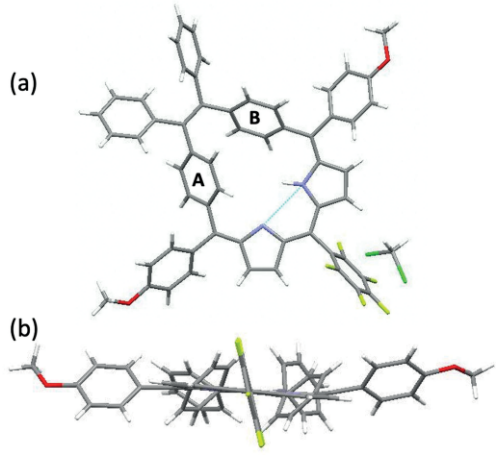

Figure 5. Top and side view of the molecular structure of compound **19** in the crystal.

Compound **20** crystallized in the monoclinic space group $P2_1/n$ (Figure 6). The crystal structure of compound **20** exhibits a similar non-planar conformation as described for compound **19**. This shows that substitution at the ethylene unit (with either Ph or Me) did not affect the conformation of the macrocyclic core. The dipyrromethene unit in **20** is twisted as compared to the one in **19**. The mean plane deviation of the atoms in the dipyrromethene unit in compound **20** is 0.036 Å while the angle between *p*-phenylene ring A and the dipyrromethene unit is 54.58(6)° [50.30(7)° for ring B].

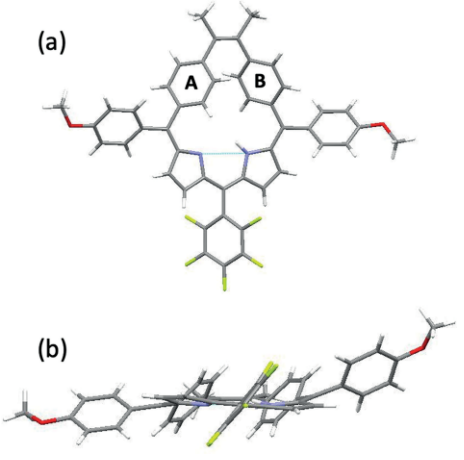

Figure 6. Top and side view of the molecular structure of compound **20** in the crystal.

Di(*m*-benzi)homoporphyrin **27** crystallized in the monoclinic space group $P2_1/c$ (Figure 7). The crystal structure analysis shows that the core is highly distorted when compared to di(*p*-benzi)homoporphyrins **19** and **20**. Additionally, the anthracene unit is almost perpendicular to the dipyrromethene unit [76.44(4)°]. The bond lengths of *m*-phenylene linkages indicate more double bond character as per the non-aromatic nature of the core. The angles between the m-phenylene rings and the dipyrromethene units are significantly larger than **19** and **20** [71.10(8)° for ring A and 52.62(6)° for ring B].

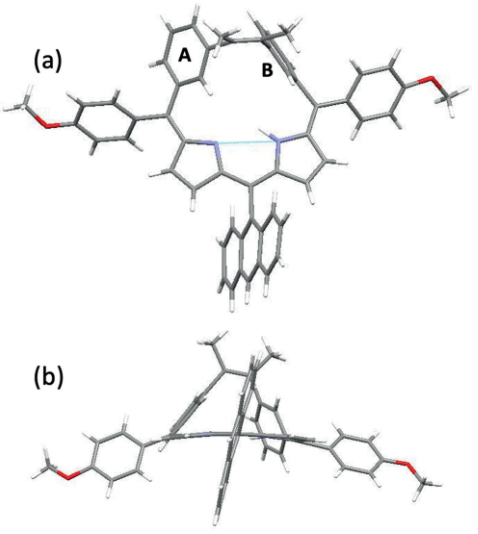

Figure 7. Top and side view of the molecular structure of compound **27** in the crystal.

Singlet Oxygen Quantum Yields

Singlet oxygen ($^1O_2$) is a key cytotoxic species generated during photodynamic therapy (PDT) for many photosensitizers. Hence, maximizing the production of $^1O_2$ within malignant tissue can enhance the therapeutic value of a PDT drug or make the photosensitizers useful in photochemical reactions.[12,18] Core-modified expanded porphyrins have been actively investigated for application to the photosensitizers. Expanded porphyrins exhibit absorption in NIR region, which is required for their use at the deepest possible tissue depths. The core modified expanded porphyrins are likely to have nonplanar skeleton and as a result triplet state quantum yield via intersystem crossing is enhanced.[19] As shown above, these homobenziporphyrins exhibited a strong absorption band between 600–700 nm. In the following, we show that they act as efficient photosensitizers for the formation of singlet oxygen.

1,3-Diphenylisobenzofuran (DPBF), acts as a singlet oxygen trap by reacting with $^1O_2$ to generate *cis*-dibenzoylbenzene.[20] Thus, we employed the use of DPBF to measure the efficiency of the synthesized compounds (**19**, **20**, **21**, **26**, **27**, and **28**). The decrease in absorbance of DPBF in the presence of di(*p*-benzi)homoporphyrins **19–21** and di(*m*-benzi)homoporphyrins **26–28** was recorded in DCM/MeOH (1:1) at a concentration of 0.13 mol L^{-1}. The same concentration of 5,10,15,20-tetraphenylporphyrin (H_2TPP) was employed to calculate the relative quantum yields (Φ_{TPP} = 0.62 in DCM).[21] The relative singlet oxygen quantum yield (Φ_{BHP}) for each of these homoporphyrins was calculated using the following equation (1):[22]

$$\Phi_{BHP} = \Phi_{TPP} \times S_{BHP}/S_{TPP} \quad (1)$$

where Φ represents quantum yield, S represents the slope, and BHP and TPP represent dibenzihomoporphyrin and 5,10,15,20-tetraphenylporphyrin, respectively.

Figure S27 and S28 represent the UV/Vis spectra of DPBF degradation in the presence of di(*p*/*m*-benzi)homoporphyrins. Figure 8 shows the decrease in DPBF absorption over time for **19**, **20**, **21**, **26**, **27**, and **28**. Determination of the singlet oxygen quantum yields in reference to H_2TPP revealed that compound **21** exhibited the lowest singlet oxygen quantum yield, whereas, compound **20** gave the highest value of quantum yield. Compound **20** exhibited the highest value of singlet oxygen quantum yield (Φ_{20} = 0.23) followed by compound **27** (Φ_{27} = 0.14), **19** (Φ_{19} = 0.12), **26** (Φ_{26} = 0.12) and **28** (Φ_{28} = 0.07). Compound **21** exhibited the lowest value of the quantum yield (Φ_{21} = 0.06) as compared to the other synthesized compounds. The potency of compounds **19** and **20** is possibly due to fluorine atom insertion to their structures which has been known to confer a high level of singlet oxygen production making them potential entities for photodynamic therapy.[23] Compound **27** has a significant singlet oxygen production due to the substitution of anthracene unit which has also been known to enhance the quantum yields with respect to singlet oxygen production.[24]

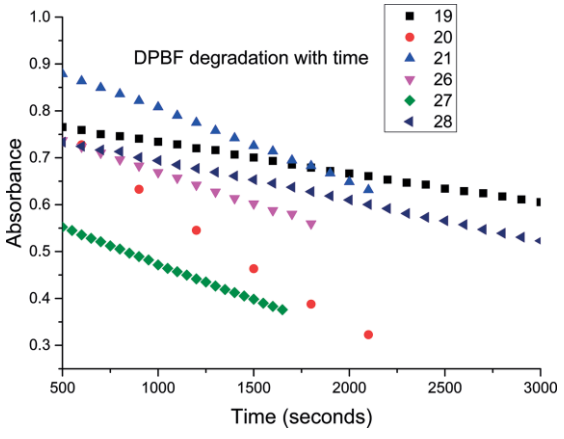

Figure 8. DPBF consumption measured at 417 nm over time for **19**, **20**, **21**, **26**, **27**, and **28** in DCM/MeOH (1:1).

Conclusion

In summary, the present study provides insight into the design of a new class of porphyrin-inspired macrocycles, i.e. di(*p*/*m*-benzi)homoporphyrins. These macrocycles were accessed using [3+1] condensation reactions between dipyrroles and aryl aldehydes. To compare the electronic properties, phenylene rings were incorporated in the macrocycle using *para*- and *meta*-linkages. In general, the compounds synthesized can be defined as an archetypical dicarbaporphyrinoid system, i.e. porphyrin surrogates with two carbon atoms and two nitrogen atoms (CCNN) in the core, containing a rigid vinylene unit at one meso-linkage. The deviation of the *m*/*p*-phenylene rings from the "mean-plane" restricted effective π-conjugation in the macrocycle leading to non-aromaticity. Structure elucidation of **19**, **20**, and **27** revealed the lack of extended π-conjugation and planarity; hence, these systems can be considered as non-aromatic macrocycles, particularly when considered alongside the results of NMR and UV/Visible spectroscopic analyses. The absorption spectra are characterized by a long-wavelength band between 600–700 nm. Additionally, singlet oxygen production could be confirmed. Further studies will evaluate potential applications in PDT and photochemistry.

Experimental Section

General Information: Condensation reactions were carried out under an argon atmosphere. Reactions involving moisture and/or air-sensitive reagents were carried out in pre-dried glassware and with standard Schlenk line techniques. All commercial reagents and anhydrous solvents were used as received from vendors (Fischer Scientific, and Sigma Aldrich). Dichloromethane (CH_2Cl_2) was dried with P_2O_5. Yields refer to chromatographically and spectroscopically (^{1}H NMR) homogeneous material unless otherwise noted. Reactions were monitored by thin-layer chromatography (TLC) and absorption spectroscopy. TLC carried out on silica gel plates. Silica gel 60 *Merck, 230–400 mesh, or aluminum oxide (Brockmann Grade I) were used for flash column chromatography. Room temperature refers to 20–25 °C.

Instrumentation: Melting points are uncorrected and were measured with a Digital Stuart SPM 10 melting point apparatus. NMR spectra were recorded using Bruker DPX400 (400 MHz for ^{1}H NMR, 101 MHz for ^{13}C NMR, 377 MHz for ^{19}F NMR), Bruker AV 600 (600 MHz for ^{1}H NMR, 151 MHz for ^{13}C NMR, 564 MHz for ^{19}F NMR), and Bruker AV 400 (400 MHz for ^{1}H NMR, 101 MHz for ^{13}C NMR, 377 MHz for ^{19}F NMR) instruments. Chemical shifts are given in ppm and referenced to the residual peak of the deuterated NMR solvent. The assignment of the signals was confirmed by 2D spectra (COSY, HMBC, HSQC). ESI mass spectra were acquired in positive or negative modes as required, using a Micromass time-of-flight mass spectrometer (TOF), or a Bruker mircoOTOF-Q II spectrometer interfaced to a Dionex UltiMate 3000 LC. APCI experiments were carried out on a Bruker microOTOF-Q III spectrometer interfaced to a Dionex Ultimate 3000 C or direct insertion probe in positive or negative modes. UV/Vis spectra were recorded in solutions using a Specord 250 spectrophotometer from Analytik Jena (1 cm path length quartz cell).

Single Crystal X-ray Crystallography: The crystals of compounds **19**, **20,** and **27** were grown following the protocol developed by Hope by dissolving the dibenzihomoporphyirns in DCM and layering with either MeOH or hexane for liquid diffusion over time.[25] Single crystal X-ray diffraction data for were collected on a Bruker APEX 2 DUO CCD diffractometer by using graphite-monochromated MoK_α (λ = 0.71073 Å) radiation (**19** and **20**) and Incoatec IμS CuK_α (λ = 1.54178 Å) (**27**) radiation. Crystals were mounted on a MiTeGen MicroMount and collected at 100(2) K by using an Oxford Cryosystems Cobra low-temperature device. Data were collected by using omega and phi scans and were corrected for Lorentz and polarization effects by using the APEX software suite.[26] Using Olex2, the structure was solved with the XT structure solution program, using the intrinsic phasing solution method and refined against $|F_2|$ with XL using least-squares minimization.[27] Hydrogen atoms were generally placed in geometrically calculated positions and refined using a riding model. Details of data refinements are mentioned in Table S1. Mercury3.7[28] and Olex2 were used for preparation of the images.[26a] Refinement details of **19**: Pyrrole hydrogen were located on the difference map and refined as semi-free with restraints (DFIX). Refinement details of **27**: Pyrrole hydrogen atoms were located on the difference map and refined using constraints (DFIX). A partially occupied DCM (40 %) was located in the void and was refined using a rigid group and restraints (SIMU).

Singlet oxygen studies: The photo-irradiation of the samples was performed in quartz cuvettes (2×1×1 cm) under irradiation via a polychromatic light source (Philips, 15V–150 W lamp), equipped with a 400 nm cut-off filter (Schott GG 400) and a 532 nm diode-pumped solid state green laser system (CW532–04, average intensity of 10 mW•cm^{-2}). The temperature of the sample was maintained at 18 °C using a Peltier element (Cary Peltier 1×1 cell holder). Relative singlet oxygen ($^1O_2$) yields (Φ_{BHP}) were calculated from the degradation slopes of the 1,3-diphenylisobenzofuran (DPBF) conversion in the presence of different photosensitizers. The absorbance of DPBF molecule was adjusted to 1.0 at 417 nm in an air-saturated solvent mixture then the corresponding photosensitizer (dibenzihomoporphyrins) was added to the solution. The solutions were irradiated form 30 min. to 1 h, and absorption spectra were recorded at t = 0 s and intervals of 100 s. A subsequent decrease in the absorbance of DPBF was observed after each irradiation. Singlet oxygen experiments were repeated twice and Φ_{BHP} values were observed in a standard deviation range of ± 0.05.

Compounds **13–18**, and **23–25** were synthesized according to procedures reported in the literature.[7b]

General Procedure 1: Dipyrrole (1.0 equiv.) was added to a solution of aryl aldehyde (1.0 equiv.) in DCM followed by addition of 1.0 equiv. of BF_3•OEt_2 or TFA. The reaction mixture was stirred at room temperature for 15 h under inert atmosphere. DDQ (3 to 3.5 equiv.) was added to the crude reaction mixture and stirred at room temperature for 1 hour in air. The solvent was removed in vacuo and the crude material was purified by basic alumina (Brockmann grade I) column chromatography.

Compound 19: Synthesized via General Procedure 1 from dipyrrole **17** (200 mg, 0.284 mmol), C_7HF_5O (56 mg, 0.284 mmol), TFA (22 µL, 0.284 mmol) and DDQ (225 mg, 0.994 mmol) in 200 mL of CH_2Cl_2. The crude material was purified by alumina column chromatography (Brockmann Grade I). Yield = 27 mg, 11 %. M.p. >300 °C; R_f = 0.77 (SiO_2, CH_2Cl_2/C_6H_{14}, 4:1, v/v); ^{1}H NMR (400 MHz, $CDCl_3$): δ = 8.00 (d, J = 8.2 Hz, 4H), 7.48 (d, J = 8.2 Hz, 4H), 7.10–7.08 (m, 6H), 7.03–6.99 (m, 8H), 6.79(d, J = 8.2 Hz, 4H), 6.46 (d, J = 5.2 Hz, 2H), 5.78 (d, J = 5.2 Hz, 2H), 3.78 (s, 6H) ppm; ^{13}C NMR (101 MHz, $CDCl_3$): δ = 160.3, 143.6, 141.4, 141.1, 138.2, 134.2, 133.7, 133.2, 132.8, 132.4, 130.9, 127.8, 127.0, 126.8, 113.3, 55.2 ppm; ^{19}F NMR (377 MHz, $CDCl_3$): δ = –138.07 (dd, J = 25.0, 8.3 Hz), –155.30 (t, J = 21.0 Hz), –161.93 (td, J = 24.7, 8.2 Hz) ppm; UV/Vis (CH_2Cl_2): λ_{max} (log ε) = 385(4.87), 653(4.25); HRMS (MALDI-TOF) m/z calcd. for $C_{57}H_{37}N_2O_2F_5$ $[M]^+$ 876.2775, found 876.2764.

Compound 20: Synthesized via General Procedure 1 from dipyrrole **18** (200 mg, 0.345 mmol), C_7HF_5O (68 mg, 0.345 mmol), TFA (26 µL, 0.345 mmol), and DDQ (240 mg, 1.06 mmol) in 200 mL of CH_2Cl_2. The crude material was purified by alumina column chromatography (Brockmann Grade I). Yield = 34 mg, 13 %. M.p. 220 °C; R_f = 0.45 (SiO_2, CH_2Cl_2/C_6H_{14}, 3:2, v/v); ^{1}H NMR (400 MHz, $CDCl_3$): δ = 7.85 (d, J = 8.0 Hz, 4H), 7.29 (d, J = 8.1 Hz, 4H), 7.01 (d, J = 8.3 Hz, 4H), 6.79 (d, J = 8.7 Hz, 4H), 6.49 (d, J = 5.1 Hz, 2H), 5.80 (d, J = 4.8 Hz, 2H), 3.79 (s, 6H), 2.04 (s, 6H) ppm; ^{13}C NMR (101 MHz, $CDCl_3$): δ = 159.7, 144.1, 137.5, 134.1, 133.9, 133.1, 132.9, 132.8, 130.3, 126.9, 113.3, 55.2, 18.5 ppm; ^{19}F NMR (376 MHz, $CDCl_3$): δ = –138.11 (dd, J = 24.9, 8.4 Hz), –155.45 (t, J = 21.0 Hz), –162.07 (td, J = 24.8, 8.5 Hz) ppm; UV/Vis (CH_2Cl_2): λ_{max} (log ε) = 376(4.71), 643(4.25); HRMS (MALDI-TOF) m/z calcd. for $C_{47}H_{33}F_5N_2O_2$ $[M]^+$ 752.2462, found 752.2463.

Compound 21: Synthesized via General Procedure 1 from dipyrrole **18** (200 mg, 0.345 mmol), C_7H_5IO (80 mg, 0.345 mmol), TFA (26 µL, 0.345 mmol), and DDQ (240 mg, 1.06 mmol) in 200 mL of CH_2Cl_2. The crude material was purified by alumina column chromatography (Brockmann Grade I). Yield = 27 mg, 10 %. M.p. charred at 270 °C; R_f = 0.66 (SiO_2, CH_2Cl_2/CH_3OH, 99:1 v/v); ^{1}H NMR (400 MHz, $CDCl_3$): δ = 7.90 (d, J = 7.3 Hz, 4H), 7.68 (d, J = 7.9 Hz, 2H), 7.03 (d, J = 7.5 Hz, 4H), 6.98 (d, J = 7.7 Hz, 4H), 6.82 (d, J = 8.6 Hz, 2H), 6.44 (d, J = 5.1 Hz, 4H), 5.96 (d, J = 4.7 Hz, 1H), 3.83 (s, 6H), 2.07 (s, 6H) ppm; ^{13}C NMR (101 MHz, $CDCl_3$): δ = 143.6, 137.3, 133.2, 132.9, 130.3, 128.7, 113.2, 55.2, 18.5 ppm; UV/Vis (CH_2Cl_2): λ_{max} (log ε) = 378(4.65), 661(4.15); HRMS (MALDI-TOF) m/z calcd. for $C_{47}H_{38}IN_2O_2$ $[M + H]^+$ 789.1978, found 789.1953.

Compound 26: Synthesized via General Procedure 1 from dipyrrole **25** (200 mg, 0.345 mmol), C_7HF_5O (68 mg, 0.345 mmol), TFA (26 µL, 0.345 mmol), and DDQ (240 mg, 1.06 mmol) in 200 mL of CH_2Cl_2. The crude material was purified by alumina column chromatography (Brockmann Grade I). Yield = 41 mg, 16 %. M.p. 212 °C; R_f = 0.4 (SiO_2, CH_2Cl_2/CH_3OH, 4:1 v/v); ^{1}H NMR (400 MHz, $CDCl_3$): δ = 7.44 (d, J = 7.5 Hz, 2H), 7.17 (d, J = 8.7 Hz, 4H), 6.97 (t, J = 7.6 Hz, 4H), 6.88 (t, J = 6.5 Hz, 6H), 6.72 (d, J = 7.9 Hz, 2H), 6.39 (d, J = 5.1 Hz, 2H), 3.84 (s, 6H), 2.05 (s, 6H) ppm; ^{13}C NMR (101 MHz, $CDCl_3$): δ = 159.8, 159.5, 148.5, 148.3, 144.5, 140.1, 135.5, 134.8, 134.0, 133.8, 131.8, 130.1, 126.8, 126.3, 126.0, 55.3, 21.0 ppm; ^{19}F NMR (377 MHz, $CDCl_3$): δ = –137.17 (dd, J = 24.9, 8.2 Hz), –138.58 (dd, J = 24.9, 8.4 Hz), –155.24 (t, J = 20.9 Hz), –161.98 to –162.37 (m) ppm; UV/Vis (CH_2Cl_2): λ_{max} (log ε) = 386(4.39), 633(4.24); HRMS (MALDI-TOF) m/z calcd. for $C_{47}H_{33}F_5N_2O_2$ $[M + H]^+$ 753.2540, found 753.1715.

Compound 27: Synthesized via General Procedure 1 from dipyrrole **25** (200 mg, 0.345 mmol), $C_{15}H_{10}O$ (72 mg, 0.345 mmol), TFA (26 µL, 0.345 mmol) and DDQ (240 mg, 1.06 mmol) in 200 mL of CH_2Cl_2. The crude material was purified by alumina column chromatography (Brockmann Grade I). Yield = 34 mg, 13 %. M.p. 192 °C; R_f = 0.60 (SiO_2, CH_2Cl_2); ^{1}H NMR (400 MHz, $CDCl_3$): δ = 8.53 (s, 1H), 8.26 (d, J = 8.6 Hz, 1H), 8.06 (d, J = 8.4 Hz, 2H), 7.95 (d, J = 8.8 Hz, 1H), 7.51–7.39 (m, 4H), 7.38–7.30 (m, 1H), 7.11 (d, J = 25.5 Hz, 5H), 6.98 (s, 2H), 6.80 (d, J = 8.3 Hz, 3H), 6.74 (s, 1H), 6.63 (d, J = 4.3 Hz, 2H), 5.82 (d, J = 3.7 Hz, 2H), 3.79 (s, 6H), 2.10 (s, 6H). ppm; ^{13}C NMR (101 MHz, $CDCl_3$): δ = 159.4, 144.5, 133.9, 133.6, 131.8, 130.1, 128.9, 126.0, 125.8, 125.6, 113.0, 55.2, 21.1 ppm; UV/Vis (CH_2Cl_2): λ_{max} (log ε) = 394(4.53), 641(4.22); HRMS (MALDI-TOF) m/z calcd. for $C_{55}H_{43}N_2O_2$ $[M]^+$ 763.3325, found 763.3291.

Compound 28: Synthesized via General Procedure 1 from dipyrrole **25** (200 mg, 0.345 mmol), C_7H_5IO (80 mg, 0.345 mmol), TFA (26 µL, 0.345 mmol), and DDQ (240 mg, 1.06 mmol) in 200 mL of CH_2Cl_2. The crude material was purified by alumina column chromatography (Brockmann Grade I). Yield = 29 mg, 11 %. M.p. 186 °C; R_f = 0.60 (SiO_2, CH_2Cl_2/CH_3OH, 99:1, v/v; 1H NMR (400 MHz, $CDCl_3$): δ = 7.78 (d, J = 8.0 Hz, 2H), 7.53 (dd, J = 19.9, 8.9 Hz, 1H), 7.45 (s, 1H), 7.26–7.16 (m, 6H), 7.10–6.96 (m, 4H), 6.94–6.82 (m, 7H), 6.75 (s, 2H), 6.58 (d, J = 5.1 Hz, 2H), 3.86 (s, 6H), 2.04 (s, 6H); ^{13}C NMR (101 MHz, $CDCl_3$): δ = 159.63, 148.89, 144.51, 137.45, 137.13, 136.85, 135.75, 134.71, 133.95, 132.78, 132.40, 131.71, 130.14, 128.47, 125.83, 113.88, 113.57, 113.18, 55.32, 20.92. ppm; UV/Vis (CH_2Cl_2): λ_{max} (log ε) = 388(4.43), 641(4.22); HRMS (MALDI-TOF) m/z calcd. for $C_{47}H_{38}IN_2O_2$ $[M]^+$ 789.1978, found 789.1957.

Supporting Information (see footnote on the first page of this article): Spectroscopic data of all compounds, singlet oxygen production measurements, and X-ray crystallographic data.

Deposition Numbers **2025181** (for **19**), **2025182** (for **20**) and **2025183** (for **27**) contain the supplementary crystallographic data for this paper. These data are provided free of charge by the joint Cambridge Crystallographic Data Centre and Fachinformationszentrum Karlsruhe Access Structures service www.ccdc.cam.ac.uk/structures.

Acknowledgments

This work was supported by grants from Science Foundation Ireland (IvP 13/IA/1894), the Irish Research Council (GOIPD/2017/1395) and has received funding from the European Union's Horizon 2020 research and innovation programme under the Marie Skłodowska-Curie Grant Agreement No. 764837. It was prepared with the support of the Technical University of Munich – Institute for Advanced Study through a Hans Fischer Senior Fellowship. Open access funding enabled and organized by Projekt DEAL.

Keywords: Expanded porphyrins · Homoporphyrins · Non-aromatic · Photosensitizer · Porphyrinoids

[1] a) A. Osuka, S. Saito, *Chem. Commun.* **2011**, *47*, 4330–4339; b) M. Toganoh, H. Furuta, *Chem. Commun.* **2012**, *48*, 937–954; c) J. L. Sessler, Z. Gross, H. Furuta, *Chem. Rev.* **2017**, *117*, 2201–2202; d) J. L. Sessler, S. J. Weghorn, *Expanded, Contracted and Isomeric Porphyrins*, Pergamon, New York, **1997**.

[2] a) R. Misra, T. K. Chandrashekar, *Acc. Chem. Res.* **2008**, *41*, 265–279; b) T. Tanaka, A. Osuka, *Chem. Rev.* **2017**, *117*, 2584–2640.

[3] a) H. Rath, J. Sankar, V. PrabhuRaja, T. K. Chandrashekar, A. Nag, D. Goswami, *J. Am. Chem. Soc.* **2005**, *127*, 11608–11609; b) J. F. Arambula, C. Preihs, D. Borthwick, D. Magda, J. L. Sessler, *Anti-Cancer Agents Med. Chem.* **2011**, *11*, 222–232; c) Z. Zhang, D. S. Kim, C.-Y. Lin, H. Zhang, A. D. Lammer, V. M. Lynch, I. Popov, O. Š. Miljanić, E. V. Anslyn, J. L. Sessler, *J. Am. Chem. Soc.* **2015**, *137*, 7769–7774.

[4] R. Grigg, *J. Chem. Soc., C* **1971**, 3664–3668.

[5] a) H. J. Callot, T. Tschamber, *Tetrahedron Lett.* **1974**, *15*, 3155–3158; b) H. J. Callot, T. Tschamber, E. Schaeffer, *Tetrahedron Lett.* **1975**, *16*, 2919–2922; c) B. Chevrier, R. Weiss, *J. Am. Chem. Soc.* **1975**, *97*, 1416–1421.

[6] a) E. Ganapathi, W.-Z. Lee, M. Ravikanth, *J. Org. Chem.* **2014**, *79*, 9603–9612; b) K. G. Thorat, G. Chowdhary, P. Isar, M. Ravikanth, *Eur. J. Org. Chem.* **2018**, *2018*, 5389–5396; c) E. Ganapathi, S. Kuilya, T. Chatterjee, M. Ravikanth, *Eur. J. Org. Chem.* **2016**, 282–290.

[7] a) K. S. Anju, M. Das, B. Adinarayana, C. H. Suresh, A. Srinivasan, *Angew. Chem. Int. Ed.* **2017**, *56*, 15667–15671; *Angew. Chem.* **2017**, *129*, 15873; b) B. Adinarayana, M. Das, C. H. Suresh, A. Srinivasan, *Chem. Eur. J.* **2019**, *25*, 4683–4687.

[8] a) M. Stępień, L. Latos-Grażyński, *Acc. Chem. Res.* **2005**, *38*, 88–98; b) T. D. Lash, *Org. Biomol. Chem.* **2015**, *13*, 7846–8082; c) D. I. AbuSalim, M. L. Merfeld, T. D. Lash, *J. Org. Chem.* **2013**, *78*, 10360–10368; d) S. C. Fosu, G. M. Ferrence, T. D. Lash, *J. Org. Chem.* **2014**, *79*, 11061–11074.

[9] T. D. Lash, S. T. Chaney, D. T. Richter, *J. Org. Chem.* **1998**, *63*, 9076–9088.

[10] a) M. Stępień, L. Latos-Grażyński, *Chem. Eur. J.* **2001**, *7*, 5113–5117; b) M. Stępień, L. Latos-Grażyński, *J. Am. Chem. Soc.* **2002**, *124*, 3838–3839.

[11] a) B. Szyszko, A. Białońska, L. Szterenberg, L. Latos-Grażyński, *Angew. Chem. Int. Ed.* **2015**, *54*, 4932–4936; *Angew. Chem.* **2015**, *127*, 5014; b) B. Adinarayana, A. P. Thomas, C. H. Suresh, A. Srinivasan, *Angew. Chem. Int. Ed.* **2015**, *54*, 10478–10482; *Angew. Chem.* **2015**, *127*, 10624.

[12] S. Callaghan, M. O. Senge, *Photochem. Photobiol. Sci.* **2018**, *17*, 1490–1514.

[13] Q. Zhao, Y. Wang, Y. Xu, Y. Yan, J. Huang, *Sci. Rep.* **2016**, *6*, 31339.

[14] a) C. J. Medforth, M. O. Senge, K. M. Smith, L. D. Sparks, J. A. Shelnutt, *J. Am. Chem. Soc.* **1992**, *114*, 9859–9869; b) M. O. Senge, *Chem. Commun.* **2006**, 243–256.

[15] X.-F. Duan, J. Zeng, J.-W. Lü, Z.-B. Zhang, *J. Org. Chem.* **2006**, *71*, 9873–9876.

[16] J. E. McMurry, M. P. Fleming, *J. Am. Chem. Soc.* **1974**, *96*, 4708–4709.

[17] a) J. M. Lim, Z. S. Yoon, J.-Y. Shin, K. S. Kim, M.-C. Yoon, D. Kim, *Chem. Commun.* **2009**, 261–273; b) R. E. Haddad, S. Gazeau, J. Pécaut, J.-C. Marchon, C. J. Medforth, J. A. Shelnutt, *J. Am. Chem. Soc.* **2003**, *125*, 1253–1268; c) S. Zakavi, N. G. Gharab, *Polyhedron* **2007**, *26*, 2425–2432.

[18] M. C. DeRosa, R. J. Crutchley, *Coord. Chem. Rev.* **2002**, *233–234*, 351–371.

[19] a) A. Harriman, B. G. Maiya, T. Murai, G. Hemmi, J. L. Sessler, T. E. Mallouk, *J. Chem. Soc., Chem. Commun.* **1989**, 314–316; b) J.-H. Ha, G. Y. Jung, M.-S. Kim, Y. H. Lee, K. Shin, Y.-R. Kim, *Bull. Korean Chem. Soc.* **2001**, *22*, 63–67.

[20] a) M. Korínek, R. Dědic, A. Molnár, A. Svoboda, J. Hála, *J. Mol. Struct.* **2005**, *744*, 727–731; b) H. Rosen, S. J. Klebanoff, *J. Biol. Chem.* **1977**, *252*, 4803–4810.

[21] J. A. S. Cavaleiro, H. Görner, P. S. S. Lacerda, J. G. MacDonald, G. Mark, M. G. P. M. S. Neves, R. S. Nohr, H.-P. Schuchmann, C. von Sonntag, A. C. Tomé, *J. Photochem. Photobiol. A* **2001**, *144*, 131–140.

[22] J. Carneiro, A. Gonçalves, Z. Zhou, K. E. Griffin, N. E. M. Kaufman, M. da G. H. Vicente, *Lasers Surg. Med.* **2018**, *50*, 566–575.

[23] T. Goslinski, J. Piskorz, *J. Photochem. Photobiol. C* **2011**, *12*, 304–321.

[24] S. Callaghan, K. J. Flanagan, J. E. O'Brien, M. O. Senge, *Eur. J. Org. Chem.* **2020**, 2735–2744.

[25] a) H. Hope, *Prog. Inorg. Chem.* **1994**, *41*, 1–19; b) M. O. Senge, *Z. Naturforsch. B* **2000**, *55*, 336–344.

[26] a) *Saint*, Version 8.37a., Bruker AXS, Inc., Madison, WI, **2013**; b) *SADABS*, version **2016**/2., Bruker AXS, Inc, Madison, WI, **2014**; c) *APEX3*, Version **2016**.9–0., Bruker AXS, Inc., Madison, WI, **2016**.

[27] a) O. V. Dolomanov, L. J. Bourhis, R. J. Gildea, J. A. K. Howard, H. Puschmann, *J. Appl. Crystallogr.* **2009**, *42*, 339–341; b) G. Sheldrick, *Acta Crystallogr., Sect. A* **2015**, *71*, 3–8.

[28] C. F. Macrae, I. J. Bruno, J. A. Chisholm, P. R. Edgington, P. McCabe, E. Pidcock, L. Rodriguez-Monge, R. Taylor, J. van de Streek, P. A. Wood, *J. Appl. Crystallogr.* **2008**, *41*, 466–470.

Received: August 25, 2020